Far and near fields of Hermite–Gaussian beams passing through an annular aperture and its numerical simulation by the angular spectrum method

Alexander TALATINIAN

Department of Optics and Photonics, Faculty of Fundamental Problems of Technology,
Wroclaw University of Technology, Wybrzeże Wyspiańskiego 27, 50-370 Wrocław, Poland;
aleksander.talatinian@pwr.edu.pl

This research focuses on the analysis of the free propagation of Hermite–Gaussian beams diffracted by a symmetrical annular aperture placed at the beam waist plane. The propagation is studied analytically and numerically using the angular spectrum method and the 2D fast Fourier transformation. Numerical simulation examples illustrate the propagation characteristics of the Hermite–Gaussian beams diffracted by an annular aperture. The beam truncation parameters and obscuration ratio influence Hermite–Gaussian beam diffraction properties.

Keywords: angular spectrum, propagation of higher modes, annular aperture, near-and far fields.

1. Introduction

Hermite–Gaussian beams (HGBs) may be treated as a physical form of eigenfunctions of the light diffraction process. The closed-form HGBs expression, which solves the paraxial Helmholtz equation regarding Cartesian coordinates and system border conditions, was first introduced by SIEGMAN [1, 2]. Since then, an interest in studying such beams has increased. LAABS studied the propagation properties of HGBs beyond the paraxial approximation [3]. SAGHAFI and SHEPPARD introduced the characteristics of standard and elegant HGBs and Laguerre–Gaussian beams (LGBs) [4]. WEN and BREAZEALE studied the diffraction beam field expressed through the complex Gaussian beam function as a base function set [5]. From then on, the technique of expansion hard-aperture functions into a finite sum of complex Gaussian functions, using the generalized diffraction integral formula has been used by many authors [6-9]. Diffraction through equilateral and isosceles right triangular apertures was also studied [10, 11]. The angular plane wave spectrum method (ASM) has been applied to calculate the propagation properties of the fundamental Gaussian mode (FGM) [12, 13], as well as to

model the propagation of the optical vortex beam (OVB) [14–19]. KIM and LEE have derived the exact electric field vector formulas for the higher order HGBs and LGBs [20]. AGRAWAL and PATTANAYAK obtained the corrections to the scalar and vector Gaussian beams (GBs) by using the ASM [21]. DUAN *et al*. obtained the vectorial Rayleigh –Sommerfeld diffraction formulas to study the propagation of HGBs and LGBs beyond the paraxial approximation [22]. ZHENG *et al*. studied the propagation of vectorial Gaussian beams behind a circular aperture by using the vectorial Rayleigh diffraction integral and the hard-edge aperture function expanded as the sum of finite-term complex Gaussian functions [23]. DUAN and LÜ presented the nonparaxial analysis of far-field properties of GBs diffracted at a circular aperture [24]. ZHOU studied the vectorial structure of the far-field of an elegant HGB by using the ASM and the method of stationary phase [25]. Recently, GU *et al*. have presented the azimuthal variant vector fields diffracted by an annular aperture based on the vectorial Rayleigh–Sommerfeld integrals under nonparaxial approximation [26].

In our presentation, the ASM algorithm is applied to the calculation of the free propagation of HGBs obstructed by an annular aperture placed centrally at the beam waist. The two-dimensional Fourier transformation (2D FT) which is applied to the ASM algorithm twice: firstly, at the stage of the initial wave field decomposition with Fourier spectrum amplitudes (then those amplitudes are multiplied by using the distance z depending on the propagation factors) and finally the 2D inverse Fourier transformation (2D IFT), which yields the wave field distribution in the observation plane. By discrete calculations of $N \times N$ fields, the AS method has been proved to be effective numerically, since both 2D FTs can be performed with the application of the fast Fourier transformation (FFT) algorithm, so in our computing the 2D FFT is combined with the AS analysis. The whole numerical procedure will be called further AS FFT method and will be applied to solve numerically the diffraction problem of various HGBs passing through annular apertures.

2. Modeling the propagation of HGBs passing through an annular aperture

Let us assume that a light beam illuminates an aperture located at $z = 0$ and then propagates in free space towards the observation plane, that is parallel to the first one and is located at $z > 0$, as shown in Fig. 1. The wave field distribution appearing behind the diffracting aperture can be calculated using the angular spectrum procedure [27]. Therefore, the wave field distribution in the observation plane is obtained by an inverse Fourier transformation of the 2D angular spectrum of the initial wave modified by the respective distance functions:

$$E_z(x, y; z) = \int\limits_{-\infty}^{+\infty}\int\limits_{-\infty}^{+\infty} \left\{ \begin{array}{l} t(x, y)E_0(v_x, v_y; z = 0)H(v_x, v_y; z) \\[2mm] \times \exp\left[2\pi i(v_x x + v_y y)\right] \end{array} \right\} \mathrm{d}v_x \mathrm{d}v_y \qquad (1)$$
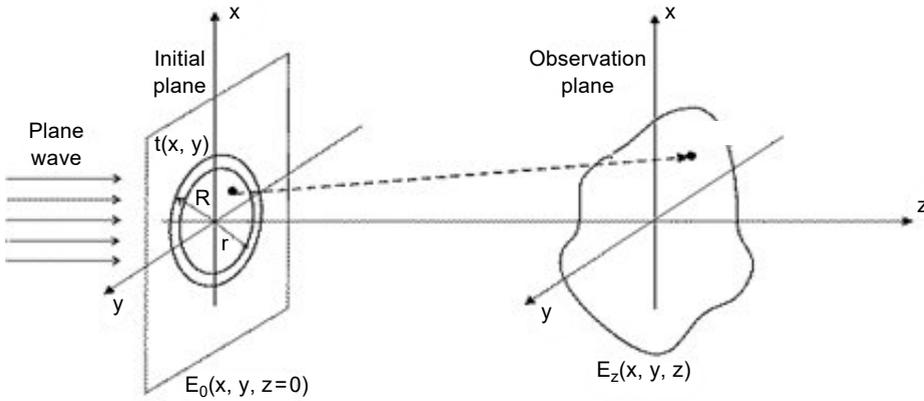
Fig. 1. Propagation of light between two parallel planes $z = 0$ and $z > 0$.

where $E_0(v_x, v_y; z = 0)$ is the initial complex amplitude spectrum defined by $E_0(v_x, v_y; z = 0) = \mathcal{F}_{2D}\{E_0(x, y; z = 0)\}$, and $k = 2\pi/\lambda$ is the wave number, λ is the wavelength of light, $t(x, y)$ is the aperture transmittance, z is the propagation distance, v_x, v_y are the spatial frequencies in Fourier domain. The distance z dependent transfer function $H(v_x, v_y; z)$ can be expressed as

$$H(v_x, v_y; z) = \exp\left[ikz\sqrt{1 - (\lambda v_x)^2 - (\lambda v_y)^2}\right] \tag{2}$$

In numerical calculations, formula (1) is converted to discrete form and all above mentioned 2D distributions are represented through respective complex valued arrays. In addition, the area of integration is not infinite, but limited to the respective squares. The calculation width of both initial and final diffraction field is D, the sampling number is $N_x \times N_y$ and the discretized spatial frequencies are $(v_x, v_y) = (p\Delta v_x, q\Delta v_y)$, where p and q are integers. Therefore, the discrete form of the Eq. (2) can be expressed as

$$H(p, q; z) = \exp\left[ikz\sqrt{1 - \lambda^2(p\Delta v_x)^2 - \lambda^2(q\Delta v_y)^2}\right] \tag{3}$$

The discretized ASM is expressed by the following equation:

$$E_z(p, q) = \text{FFT}_2^{-1}\{\text{FFT}_2\{E_0(i, j)\} t(p, q) H(p, q)\} \tag{4}$$

In the Cartesian coordinate system, the hard annular aperture function is written as

$$t(x, y) = \begin{cases} 1, & r^2 \leq x^2 + y^2 \leq R^2 \\ 0, & r^2 > x^2 + y^2 > R^2 \end{cases} \tag{5}$$

where R and r are the outer and inner radius of the annular aperture, respectively. Assume that, as shown in Fig. 1, an annular aperture, located at the plane $z = 0$ is illumi-

nated from the left by a HGB that is symmetric and with a waist plane also at $z = 0$. It is assumed that the beam is well oriented with respect to the coordinate system and can be described at $z = 0$ by H_{mn} function. The complex amplitude distribution of the wave field just behind the annular aperture ($z = 0$) is given then by

$$E_0(x, y, z = 0) = E_0 t(x, y) H_m\left(\frac{\sqrt{2}\,x}{W_0}\right) H_n\left(\frac{\sqrt{2}\,y}{W_0}\right) \exp\left(-\frac{x^2 + y^2}{W_0^2}\right) \tag{6}$$

Here, H_m and H_n are the Hermite polynomials of orders m and n in the x and y directions, respectively, W_0 is the radius at the beam waist, and E_0 is the electric field amplitude.

The FT of $E_0^{\text{HG}}(x, y; z = 0)$ has the expression

$$E_0(v_x, v_y; z = 0) = \int_{-\infty}^{+\infty}\int_{-\infty}^{+\infty}\left\{ \begin{matrix} E_0 H_m\left(\dfrac{\sqrt{2}\,x}{W_0}\right) H_n\left(\dfrac{\sqrt{2}\,y}{W_0}\right) \exp\left(-\dfrac{x^2 + y^2}{W_0^2}\right) \\ \times \exp\left[-2\pi i(v_x x + v_y y)\right] \end{matrix} \right\} dx\, dy \tag{7}$$

The complex amplitude distribution at the observation plane, derived from (1) can be written in the form

$$E_z(x, y; z) = \int_{-\infty}^{+\infty}\int_{-\infty}^{+\infty}\left\{ \begin{matrix} t(x, y) E_0(v_x, v_y; z = 0) \\ \times \exp\left[ikz\sqrt{1 - (\lambda v_x)^2 - (\lambda v_y)^2}\right] \\ \times \exp\left[2\pi i(v_x x + v_y y)\right] \end{matrix} \right\} dv_x dv_y \tag{8}$$

3. Numerical simulation results and analyses

The closed form of the diffracted HGBs passing through an annular aperture was performed using Eq. (8) and constitutes the reference for all comparisons. The AS FFT algorithm evaluation is the main numerical simulation applied in this paper. From Eq. (8) we can see that the general propagation properties of HGBs diffracted by an annular aperture depend on a few geometrical and physical factors, such as the width of the beam waist W_0, wavelength λ of the light, the propagation distance z, the mode number n, m, the inner r and the outer R radii of the annular aperture. We introduce the outer truncation parameter $\delta_R = R/W_0$, the inner truncation parameter $\delta_r = r/W_0$ and the obscuration ratio of the annular aperture $\varepsilon = r/R$.

3.1. Advantages of the angular spectrum algorithm

In the ASM approach, a wave field is treated as a superposition of planar waves. Due to that, AS FFT algorithm can cover very short distances up to $z < \lambda$, while for the Fresnel diffraction integrals, the minimal distance is $z \gg D$. This method also has the

advantage of the calculation speed due to the use of 2D FFT. Discrete form of Eq. (8) is extremely computationally efficient and is very fast when a 2D FFT algorithm can be applied here twice. Let us assume that in the discrete version of the AS diffraction integrals Eq. (8) the sampling number of mesh points on both the initial and the observation planes is N. The same is the sampling number of mesh point planes in the 2D spatial frequency space. For 1D FT, the total sampling number of required operations is reduced by the application of the FFT from $O(N^2)$, in the case of the straightforward method to $O(N^2 \log_2 N)$ for the radix-2 complex FFT algorithm. In the case of 2D FFT, the estimated saving in the computation is in the order of the square of the above and for example by $N = 1024$ calculation time is shortened by more than 10^4 times. Earlier results of the AS FFT algorithm method verified its quality [28].

3.2. Basic limitations of the AS FFT algorithm

Besides, such as the computational advantages when a 2D FFT algorithm is used, the numerical implementation of the AS FFT algorithm has several drawbacks, which are related to the limited dimensions of integration and discrete sampling taken in the initial and in the observation planes and in the spatial frequency domain. However, the ASM is prone to a serious problem, in that it causes strong aliasing errors in longer distance propagation. In the 2D discrete Fourier transform calculations, the wave field is sampled at $N_x \times N_y$ points ($p\Delta x, q\Delta y$), where $p = -N_x/2 + 1, \ldots, N_x/2, q = -N_y/2 + 1, \ldots, N_y/2$ and the 2D FFT procedure leads to an array of complex Fourier amplitudes at $N_x \times N_y$ points ($p\Delta v_x, q\Delta v_y$), where Δv_x and Δv_y are the spatial frequency domain which is equal to $\Delta v_x = 1/D_x$ and $\Delta v_y = 1/D_y$. Assuming $N = N_x = N_y$ a full representation of the initial plane requires a complex valued array of $N \times N$ and the calculation width of the diffraction field is $D = D_x = D_y = 1/\Delta v$. Considering both direct and inverse 2D FFT algorithms, one has to remember about the consequences of the sampling theorem that causes that the final result has a periodic nature with the period $D = N\Delta v$. In the case, when the calculated beam diameter approaches the value of that period, the field overlapping at the edges occurs, causing the interference between neighboring periods and leading to false fringes that are visible in Figs. 2(b) and (c). This is due to the fact that the propagation factor in Eq. (8) changes rapidly in the spatial frequency space, and those changes overcome the respective sampling limit criteria, leading to aliasing effects in the output field after the inverse FT is performed. This point is illustrated in Fig. 2 that shows an effect of aliasing on the axial intensity distributions of a finite-size of diffracted HGB passing through an annular aperture.

3.3. The intensity distributions on-axis *x* and on-axis *y* in the near and the far fields

The examples of the 2D transverse intensity distributions (left column), normalized axial intensity distribution on-axis *x* (center column) and on-axis *y* (right column) of several HG$_{mn}$ modes passing through an annular aperture are presented in Fig. 3. As can be seen in the middle figures that the normalized on-axis intensity distributions
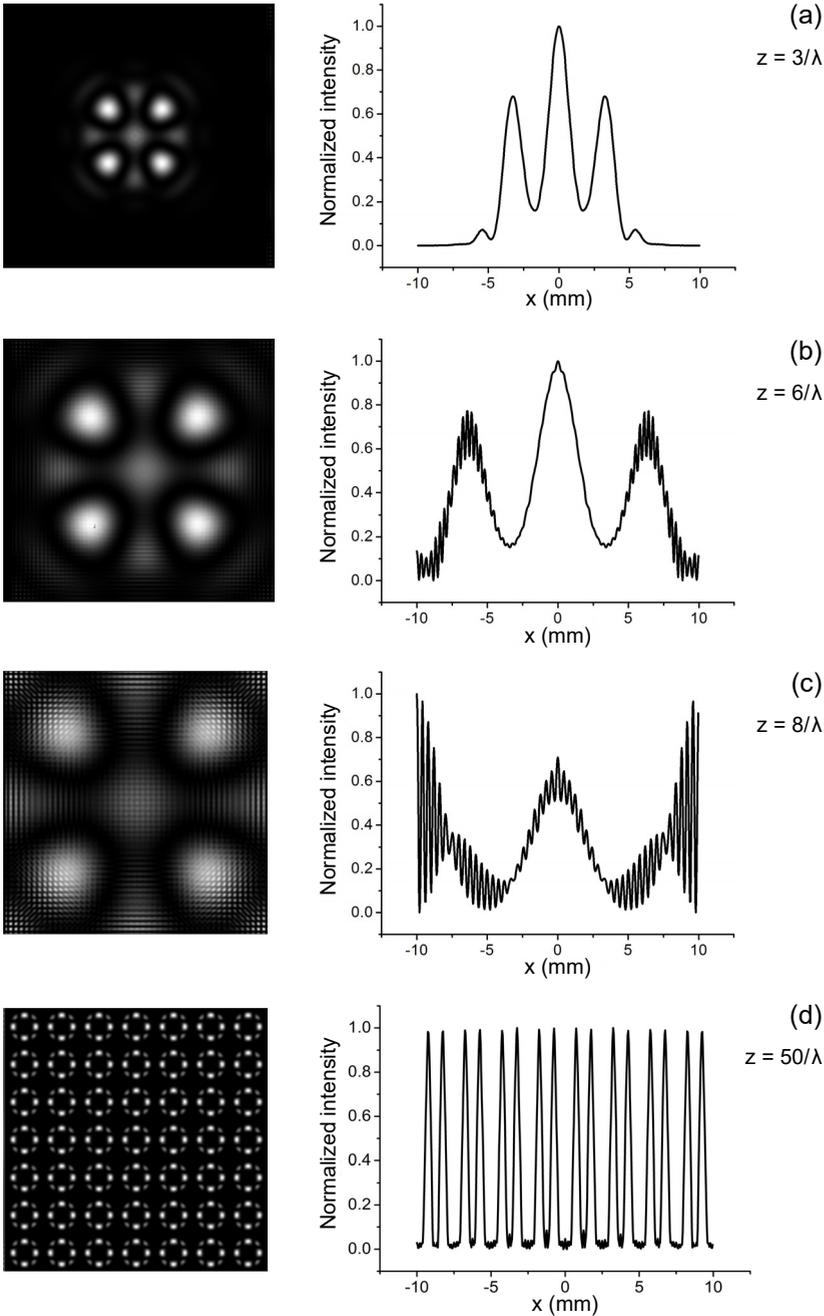
Fig. 2. AS FFT calculations of the HG_{44} mode passing through an annular aperture. The transverse cross-sectional intensity distribution (first column), and normalized axial intensity distributions along on-axis x (second column). Calculations are performed for $W_0 = 1$ mm, $D = 20$ mm, $\lambda = 0.001$ mm, $R = 1$ mm, and $r = 0.5$ mm. The effect of aliasing that occurs at longer distances results in the fringes visible in (b) and (c).
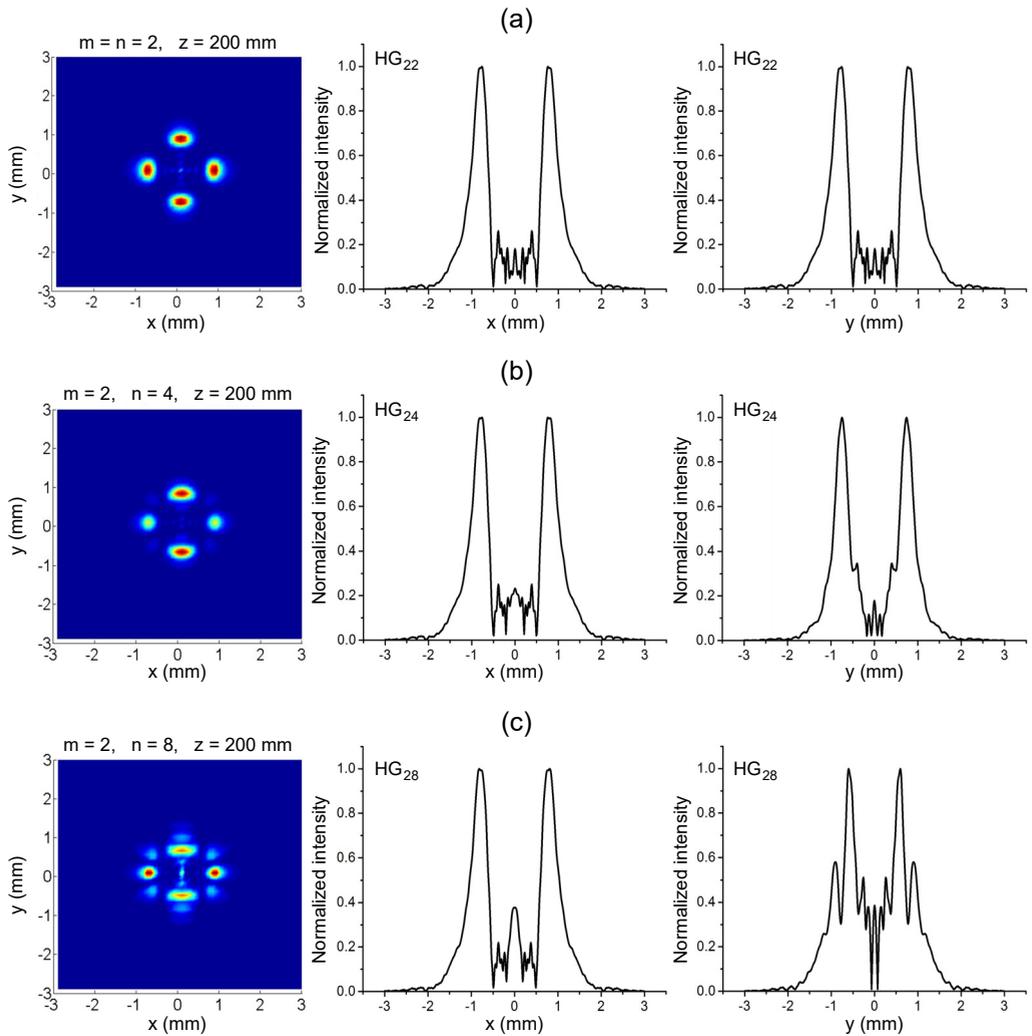
Fig. 3. Transversal intensity distribution of several HGB modes (a) HG_{22}, (b) HG_{24}, and (c) HG_{28} passing through an annular aperture in the near-field region (left column), the normalized axial intensity distributions along on-axis x (central column), and on-axis y (right column). The numerical simulation uses the AS FFT algorithm with $z = 200$ mm, $W_0 = 1$ mm, $\lambda = 632.8$ nm, $R = 1$ mm, and $r = 0.5$ mm.

for the three different modes HG_{22}, HG_{24}, and HG_{28} are nearly the same in the x direction, but are different in the y direction (right column). One can see that the on-axis intensity distribution changes in different modes.

The transversal intensity and the normalized axial intensity distributions for several HG_{mn} modes passing through an annular aperture are depicted in Fig. 4. Comparing Figs. 3 and 4, one can see that in the near-field region, the diffraction patterns of the on-axis intensity distribution both vary in different modes. However, in the far-field
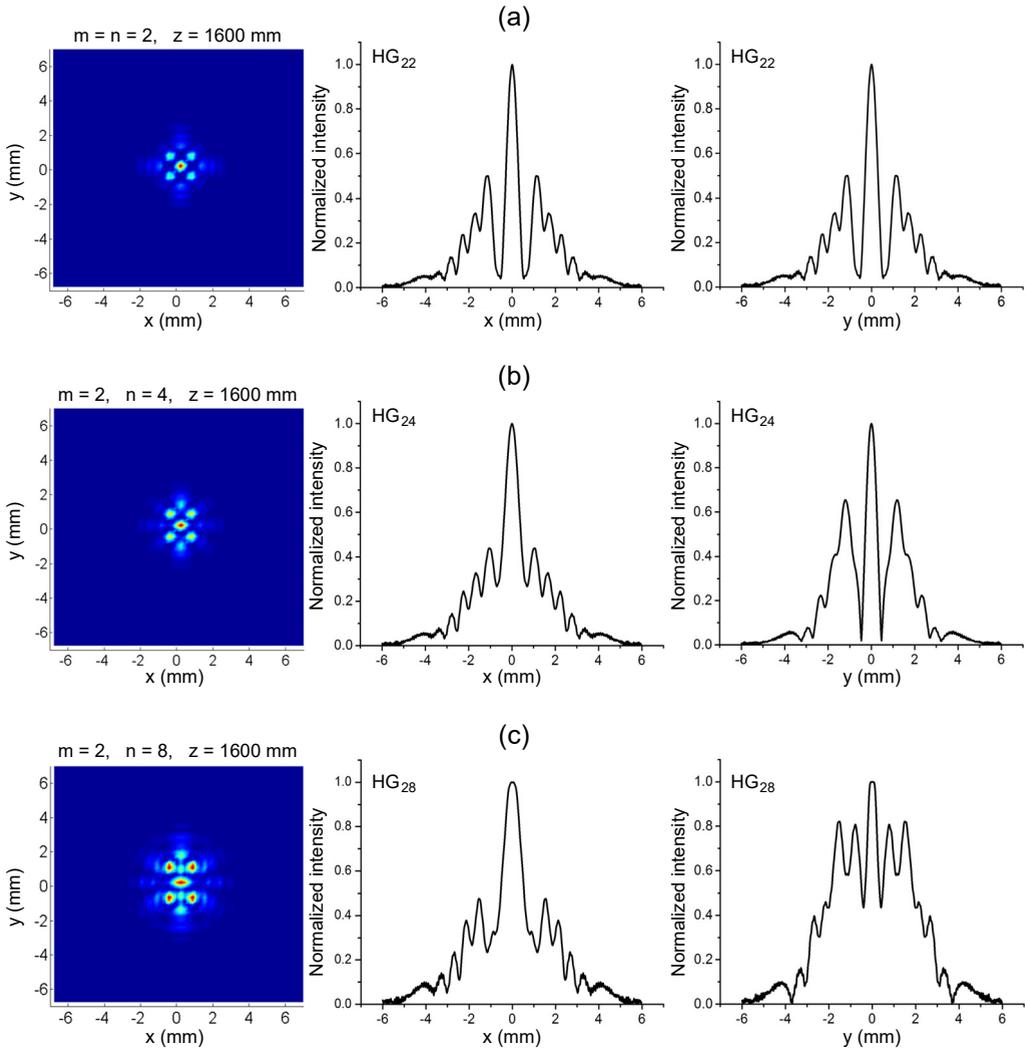
Fig. 4. Transversal intensity distribution of several HGB modes (a) HG_{22}, (b) HG_{24}, and (c) HG_{28} passing through an annular aperture in the far-field region (left column), the normalized axial intensity distribution along on-axis x (center column), and on-axis y (right column). Calculation are performed for $z = 1600$ mm, $W_0 = 1$ mm, $\lambda = 632.8$ nm, $R = 1$ mm, and $r = 0.5$ mm.

region, the diffraction pattern is invariant, the on-axis intensity distribution is varying in the x direction, whereas the diffraction pattern for the on-axis intensity is very different in the y direction.

3.4. The on-axis intensity distribution as a function of the propagation distance z

The results of the numerical calculations were performed by using Eq. (8) to illustrate the evolution of on-axis intensity distribution passing through an annular aperture and
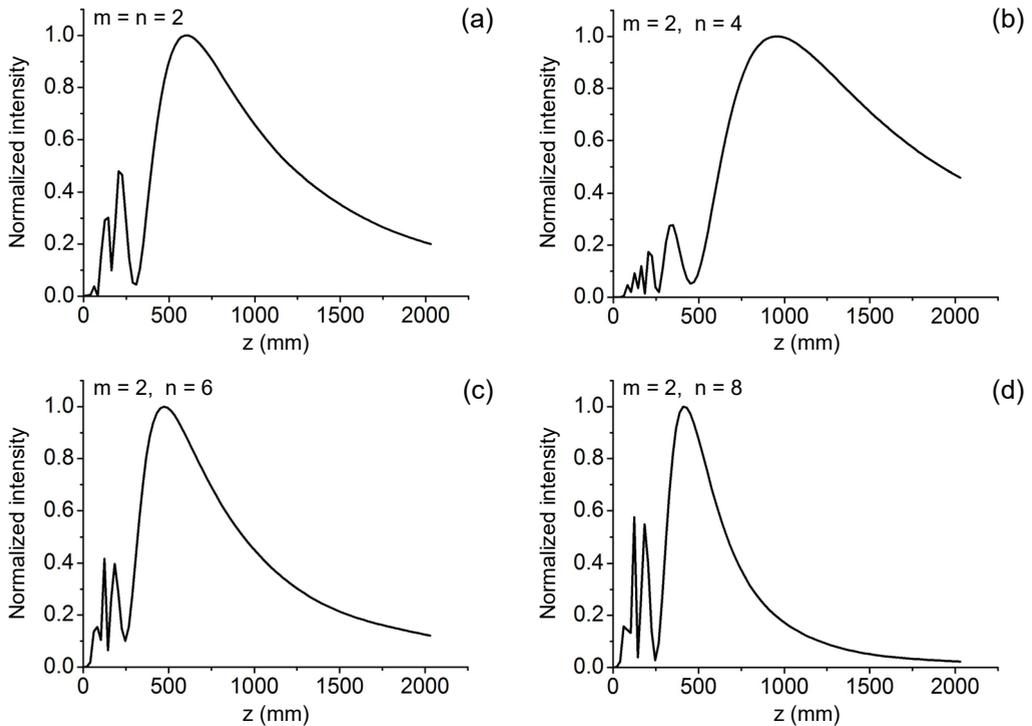
Fig. 5. The normalized axial intensity distributions as a function of the propagation distance z for several HGB modes (a) HG_{22}, (b) HG_{24}, (c) HG_{26}, and (d) HG_{28} passing through an annular aperture. The numerical simulation uses the AS FFT algorithm with $W_0 = 1$ mm, $\lambda = 632.8$ nm, $R = 1$ mm, and $r = 0.5$ mm.

to stress, the influence of aperture diffraction on the changes in the beam shape intensity of the HGBs from near-field to the far-field regions are shown in Fig. 5. The normalized on-axis intensity distribution causes fierce and fast oscillations in the near-field region. Because of the interference between the two-edge, the diffracted waves increase throughout the near-field. Whereas the oscillations of diffraction patterns disappear clearly in the far-field region, and the change of diffraction tends to stability. As it is visible in Fig. 5, the on-axis intensity distribution patterns for four different H_{mn} modes are nearly the same, and only the difference in intensity magnitudes exists.

3.5. The transverse intensity and the phase distributions with different truncation parameters

The results of the numerical calculation model of the transverse intensity and phase distributions are obtained using the AS FFT algorithm, which uses the 2D FFT procedure. It has been divided into three steps: first, determining the intensity and phase distributions of the HGB; second, calculating the intensity and phase distribution of the HGB diffracted by an annular aperture starting at the initial plane, *i.e.* the location of the minimum waist ($z = 0$), which is called a diffracting aperture; and third, calculating
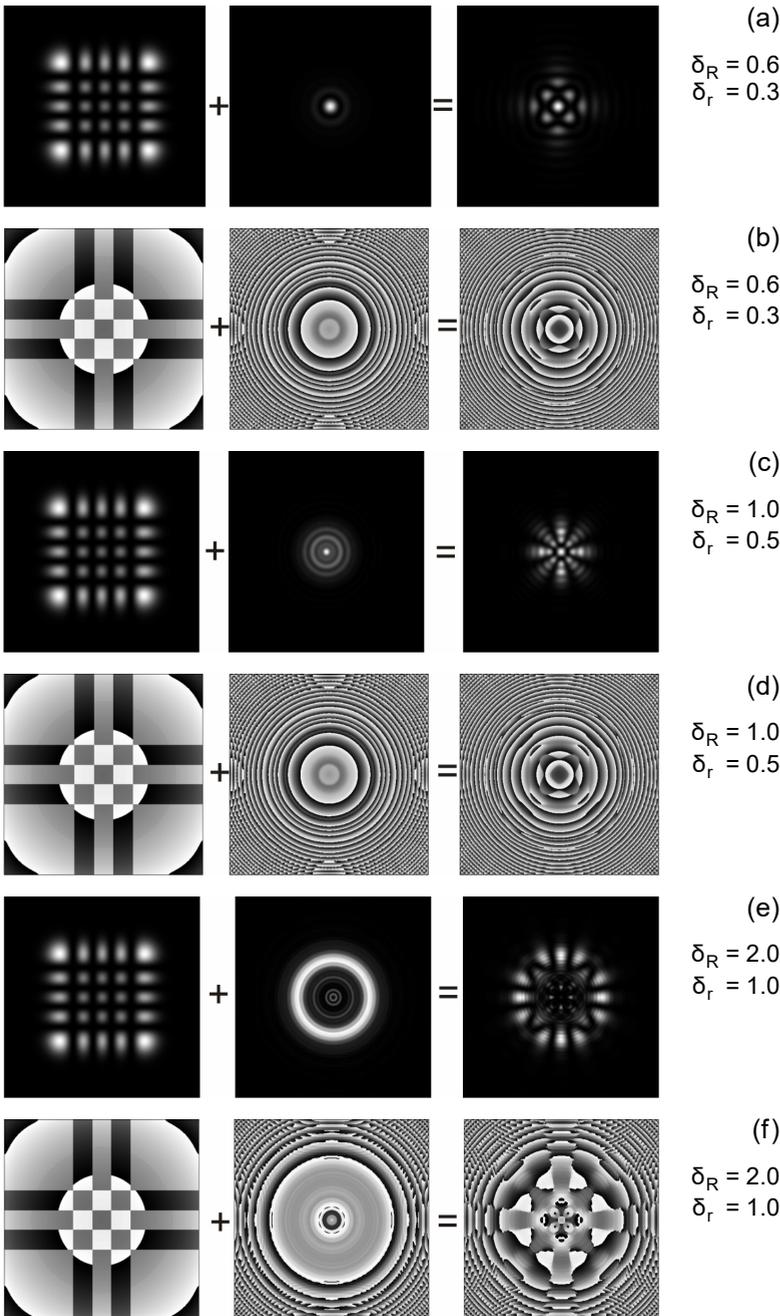
Fig. 6. A combination of the transverse intensity and phase distributions of the HG_{44} mode (left column) plus a diffracting aperture (middle column), which can produce a diffraction pattern (right column) of the HGB diffracted by an annular aperture at the observation plane $z = 200$ mm, for a fixed obscuration ratio $\varepsilon = 0.5$ and for different values of outer and inner beam truncation parameters $\delta_R = 0.6$ (a,b), $\delta_R = 1$ (c,d), $\delta_R = 2$ (e,f), and $\delta_r = 0.3$ (a,b), $\delta_r = 0.5$ (c,d), $\delta_r = 1$ (e, f), respectively. The size of each picture is 4 mm.

the propagation of the HGB diffracted by the aperture between the initial and the observation planes, which is a sum of the freely propagating HGB and a beam multiplied by the diffracting aperture as are shown in Fig. 6. It is clear from figures that the transverse intensity in a cross-section plane and the phase distribution of HGBs diffracted by passing through an annular aperture are depending strongly on the beam truncation parameters, which have influences on the beam shape intensity and the phase distributions. In addition, the beam truncation parameters influence the beam diffraction.

3.6. The beam truncation parameters effect on axial intensity distribution

Figure 7 shows the normalized axial intensity distribution of the HGB passing through an annular aperture as a function of the propagation distance z. For comparison, the result for the unapertured (without aperture) case is also shown (black curve). The maxima and minima of these oscillations are due to the interference between the two edge-diffracted waves increasing throughout in the near-field region. As it is visible in Fig. 7, the strength of the oscillation increases as the beam truncation parameter decreases, and the maximum of intensity shifts towards the aperture as the beam truncation parameter decreases.
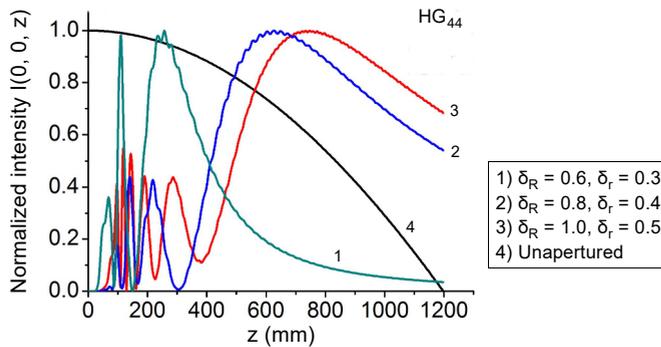

Fig. 7. The normalized axial intensity distribution as a function of the propagation distance z for HG_{44} modes passing through an annular aperture. Calculations are performed for a fixed obscuration ratio parameter ε and for different values of beam truncation parameters $\delta_R = 0.6$, 0.8, and 1 and $\delta_r = 0.3$, 0.4, and 0.5, respectively. In the calculations we take $W_0 = 1$ mm, $\lambda = 632.8$ nm.

3.7. On-axis and off-axis intensity distributions in the near and far fields

Simulation results of numerical implementation of Eq. (8) for the transverse cross-sectional intensity distributions of several HG_{mn} modes and its propagation 2D and 3D at different propagation distance z, are shown in Figs. 8 and 9. As can be seen that the transversal intensity distributions along the corresponding axes for different HG_{mn} modes have a certain proportion of the HG_{mn} mode, when the mode order is even, HG_{24} and HG_{44}, as shown in Figs. 8(a) and (b). When the mode order is odd HG_{23} in Fig. 8(c), the transverse intensity along the corresponding axis is 0, which is the dark
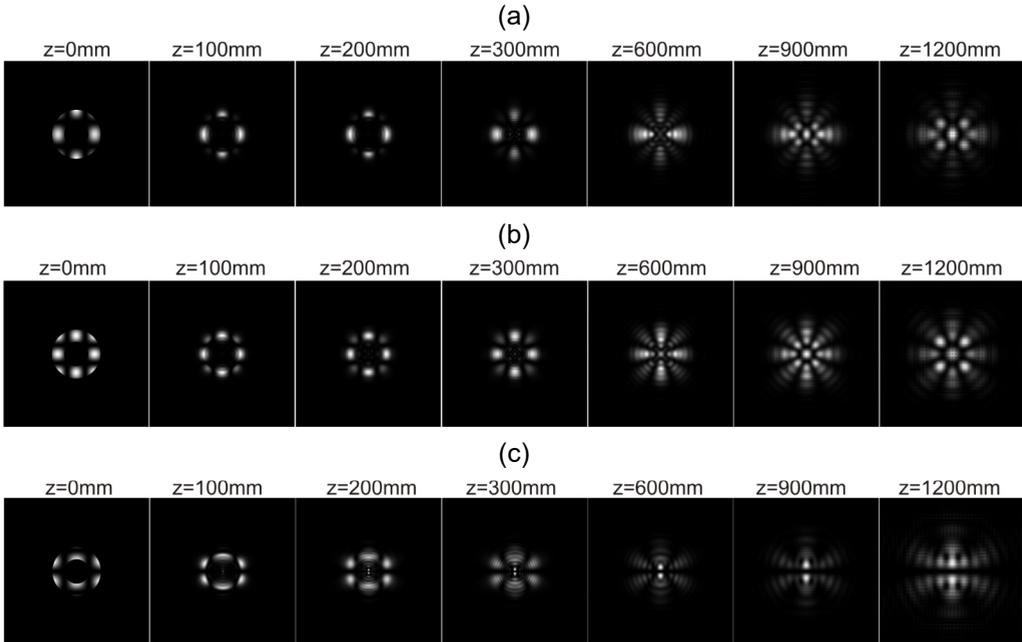
(a)

(b)

(c)

Fig. 8. AS FFT calculations of the HG_{mn} modes passing through an annular aperture at different observation planes, showing the transverse intensity distribution in a plane cross-section (a, b, c), the size of each picture is 6 mm. Calculations are performed for $\lambda = 632.8$ nm, $W_0 = 1$ mm, $R = 1$ mm, and $r = 0.5$ mm.

fringe. In the figures, we find that the transverse intensity distribution changes quickly with changing propagation distance z. The comparison of the plots in these figures shows variations of the transverse intensity diffraction distributions with the propagation distance z from near-field to far-field regions for different HG_{mn} modes. As can be clearly seen in Figs. 9(a) and (b), the diffraction axial intensity increases in the near-field just behind the annular aperture, and shows fast oscillations, then the axial intensity decreases rapidly with the increase in the propagation distance. Moreover, the HGB seems to bifurcate and two diffraction side lobes appear beside the central beam. With the increase in the propagation distance and the brighter spots can be seen in Figs. 9(a) and (b). These bright spots result from the constructive and destructive interference of the two edge-diffracted waves. Figure 9(c) shows the off-axis intensity distribution decreases in the near-field behind the annular aperture, but the intensity increases gradually with the propagation distance and then decreases, and the bright spots can be seen. A comparison of the on-axial and off-axial intensity distribution along the propagation direction shows that there is the same oscillation in the on-axial and in the off-axial intensity distributions, but the locations of the maxima and the minima are different. From the results in Figs. 8 and 9, we can see that the diffraction intensity changes along the propagation distance z and differs for different HG_{mn} modes.
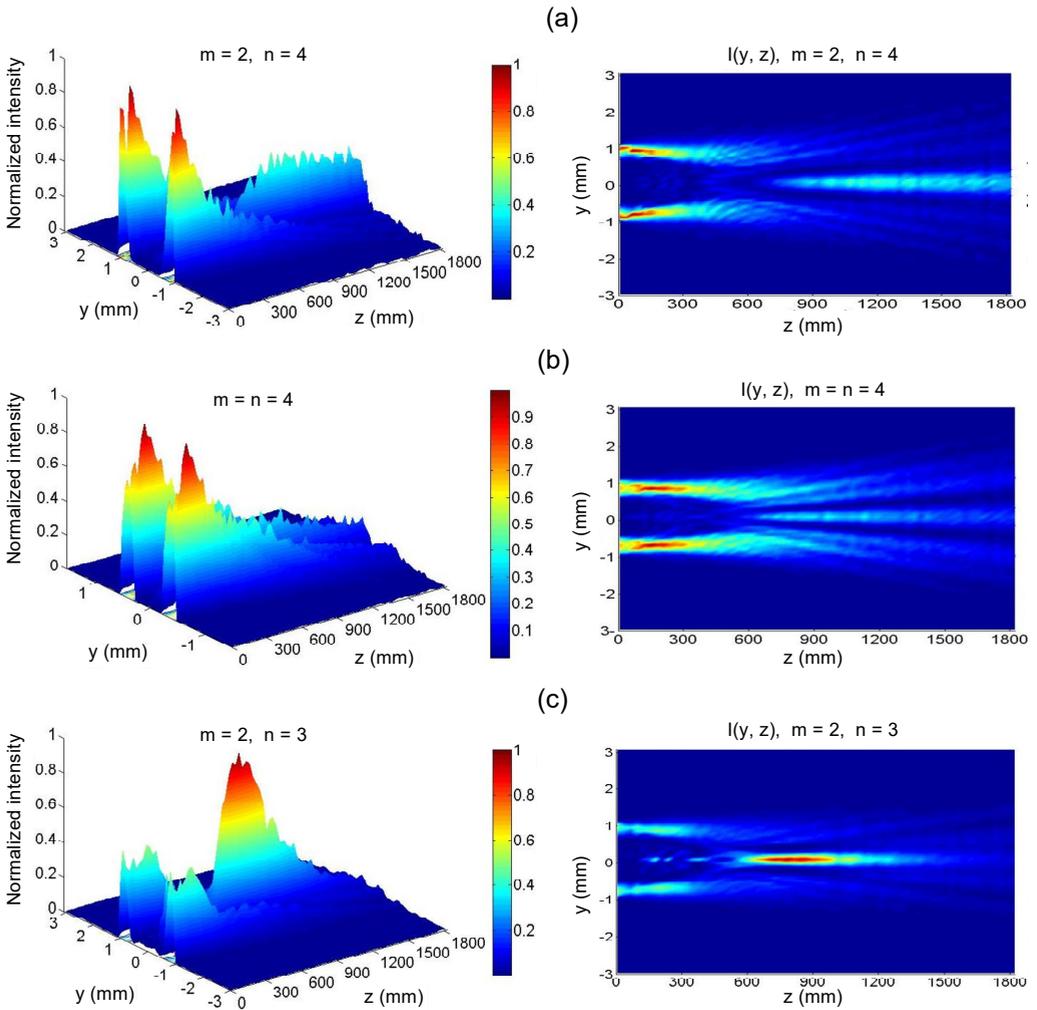
(a)

(b)

(c)

Fig. 9. The 2D and 3D propagation of the axial intensity distribution profiles in the sagittal plane (a, b) and in the off- axis direction, where $x = y = 2$ mm (c). Calculations are performed for $\lambda = 632.8$ nm, $W_0 = 1$ mm, $R = 1$ mm, and $r = 0.5$ mm. Red color represents the maximum intensity, and blue color represents the minimum intensity.

4. Conclusions

The numerical model for evaluating the diffraction patterns of the HGBs passing through an annular aperture has been introduced by using FFTs and AS methods. The AS FFT algorithm was used to calculate the complex amplitude with its real part, the transverse intensity, longitudinal intensity, and phase distributions by using a computational program written in Borland C++Builder. The images are processed in Borland C++ Build-

er to reduce the noise and adjust the brightness and contrast. The obscuration ratio and the beam truncation parameters have a significant influence on the transverse intensity, the longitudinal intensity, as well as the phase distributions, which originate from the diffraction effect caused by an annular aperture. The applied method significantly improves the numerical efficiency and reduces the computation effort significantly. Furthermore, the AS FFT algorithm can be applied in the full distance range without restriction on the far field. AS FFT algorithm may be extended to model the vector EM field and beyond the paraxial limitations and can be very useful in modeling in many other problems like computer generated holograms, optical tweezing, optical communication, optical vortices, *etc*.

References

[1] SIEGMAN A.E., *Lasers*, Oxford University Press, Mill Valley, CA 1986.

[2] SIEGMAN A.E., *Hermite–Gaussian functions of complex argument as optical-beam eigenfunctions*, Journal of the Optical Society of America **63**(9), 1973: 1093-1094. https://doi.org/10.1364/JOSA.63.001093

[3] LAABS H., *Propagation of Hermite–Gaussian-beams beyond the paraxial approximation*, Optics Communications **147**(1-3), 1998: 1-4. https://doi.org/10.1016/S0030-4018(97)00607-X

[4] SAGHAFI S., SHEPPARD C.J.R., *Near and far field of elegant Hermite–Gaussian and Laguerre–Gaussian modes*, Journal of Modern Optics **45**(10), 1998: 1999-2009. https://doi.org/10.1080/09500349808231738

[5] WEN J.J., BREAZEALE M.A., *A diffraction beam field expressed as the superposition of Gaussian beams*, The Journal of the Acoustical Society of America **83**(5), 1988: 1752-1756. https://doi.org/10.1121/1.396508

[6] ZHENG C., *Propagation of elliptical Gaussian beam passing through aperture paraxial optical systems*, Optik **125**(1), 2014: 264-267. https://doi.org/10.1016/j.ijleo.2013.06.053

[7] TANG B., JIANG X.F., LIU Z.M., *Propagation of Hermite-cosh-Gaussian beams passing through ABCD optical system with an annular aperture*, Optoelectronics Letters **4**(1), 2008: 78-80. https://doi.org/10.1007/s11801-008-7116-5

[8] ZHENG C., ZHANG Y., WANG L., *Propagation of vectorial Gaussian beams behind a circular aperture*, Optics & Laser Technology **39**(3), 2007: 598-604. https://doi.org/10.1016/j.optlastec.2005.10.003

[9] CAI Y., LÜ X., *Propagation of Bessel and Bessel–Gaussian beams through unapertured or aperture misaligned paraxial optical systems*, Optics Communications **274**(1), 2007: 1-7. https://doi.org/10.1016/j.optcom.2007.01.058

[10] BAHL M., SENTHILKUMARAN P., *Energy circulation in singular beams diffracted through an isosceles right triangular aperture*, Physical Review A **92**(1), 2015: 013831. https://doi.org/10.1103/PhysRevA.92.013831

[11] BHARGAVA RAM B.S., SHARMA A., SENTHILKUMARAN P., *Diffraction of V-point singularities through triangular apertures*, Optics Express **25**(9), 2017: 10270-10275. https://doi.org/10.1364/OE.25.010270

[12] TALATINIAN A., *Numerical simulation of the physical properties of Gaussian mode using the angular spectrum technique*, Optik **127**(17), 2016: 6970-6977. https://doi.org/10.1016/j.ijleo.2016.05.009

[13] TALATINIAN A., *The analysis of the laser beam shape of the fundamental Gaussian mode by testing the numerical angular spectrum technique*, Optics & Laser Technology **118**, 2019: 75-83. https://doi.org/10.1016/j.optlastec.2019.05.001

[14] GHAI D.P., SENTHILKUMARAN P., SIROHI R.S., *Single-slit diffraction of an optical beam with phase singularity*, Optics and Lasers in Engineering **47**(1), 2009: 123-126. https://doi.org/10.1016/j.optlaseng.2008.07.019

[15] SINGH B.K., MEHTA D.S., SENTHILKUMARAN P., *Visualization of internal energy flows in optical fields carrying a pair of fractional vortices*, Journal of Modern Optics **60**(13), 2013: 1027-1036. https://doi.org/10.1080/09500340.2013.828790

[16] LOCHAB P., SENTHILKUMARAN P., KHARE K., *Near-core structure of a propagating optical vortex*, Journal of the Optical Society of America A **33**(12), 2016: 2485-2490. https://doi.org/10.1364/JOSAA.33.002485

[17] POPIOŁEK-MASAJADA A., SOKOLENKO B., AUGUSTYNIAK I., MASAJADA J., KHOROSHUN A., BACIA M., *Optical vortex scanning in an aperture limited system*, Optics and Lasers in Engineering **55**, 2014: 105-112. https://doi.org/10.1016/j.optlaseng.2013.10.023

[18] PŁOCINICZAK Ł., POPIOŁEK-MASAJADA A., SZATKOWSKI M., WOJNOWSKI D., *Transformation of the vortex beam in the optical vortex scanning microscope*, Optics & Laser Technology **81**, 2016: 127-136. https://doi.org/10.1016/j.optlastec.2016.01.040

[19] PŁOCINICZAK Ł., POPIOŁEK-MASAJADA A., MASAJADA J., SZATKOWSKI M., *Analytical model of the optical vortex microscope*, Applied Optics **55**(12), 2016: B20-B27. https://doi.org/10.1364/AO.55.000B20

[20] KIM H.C., LEE Y.H., *Hermite–Gaussian and Laguerre–Gaussian beams beyond the paraxial approximation*, Optics Communications **169**, 1999: 9-16. https://doi.org/10.1016/S0030-4018(99)00411-3

[21] AGRAWAL G.P., PATTANAYAK D.N., *Gaussian beam propagation beyond the paraxial approximation*, Journal of the Optical Society of America **69**(4), 1979: 575-578. https://doi.org/10.1364/JOSA.69.000575

[22] DUAN K., WANG B., LÜ B., *Propagation of Hermite–Gaussian and Laguerre–Gaussian beams beyond the paraxial approximation*, Journal of the Optical Society of America A **22**(9), 2005: 1976-1980. https://doi.org/10.1364/JOSAA.22.001976

[23] ZHENG C., ZHANG Y., WAN L., *Propagation of vectorial Gaussian beams behind a circular aperture*, Optics & Laser Technology **39**(3), 2007: 598-604. https://doi.org/10.1016/j.optlastec.2005.10.003

[24] DUAN K., LÜ B., *Nonparaxial analysis of far-field properties of Gaussian beams diffracted at a circular aperture*, Optics Express **11**(13), 2003: 1474-1480. https://doi.org/10.1364/OE.11.001474

[25] ZHOU G., *Vectorial structure of the far field of an elegant Hermite–Gaussian beam*, Optics & Laser Technology **44**(1), 2012: 218-225. https://doi.org/10.1016/j.optlastec.2011.06.022

[26] GU B., XU D., PAN Y., CUI Y., *Nonparaxial propagation and focusing properties of azimuthal-variant vector fields diffracted by an annular aperture*, Journal of the Optical Society of America A **31**(7), 2014: 1657-1665. https://doi.org/10.1364/JOSAA.31.001657

[27] GOODMAN J.W., *Introduction to Fourier Optics*, 3rd Ed., Roberts & Company, Greenwood Village, 2005.

[28] TALATINIAN A., PLUTA M., *Propagation of a fundamental laser mode and its numerical simulation by the angular spectrum technique*, Optik **127**(8), 2016: 3882-3887. https://doi.org/10.1016/j.ijleo.2016.01.111